PHOTONICS Research

Integration of nanoscale light emitters: an efficient ultraviolet and blue random lasing from $NaYF_4$:Yb/Tm hexagonal nanocrystals

Ya-Pei Peng,[1] Wei Lu,[2] Pengpeng Ren,[1] Yiqun Ni,[1] Yunfeng Wang,[3] Long Zhang,[4] Yu-Jia Zeng,[1] Wenfei Zhang,[1,5] and Shuangchen Ruan[1,6]

[1]Shenzhen Key Laboratory of Laser Engineering, Key Laboratory of Advanced Optical Precision Manufacturing Technology of Guangdong Higher Education Institutes, College of Optoelectronic Engineering, Shenzhen University, Shenzhen 518060, China
[2]University Research Facility in Materials Characterization and Device Fabrication, The Hong Kong Polytechnic University, Hong Kong 999077, China
[3]Department of Applied Physics, The Hong Kong Polytechnic University, Hong Kong 999077, China
[4]Key Laboratory of Materials for High Power Laser, Shanghai Institute of Optics and Fine Mechanics, Chinese Academy of Sciences, Shanghai 201800, China
[5]e-mail: zhangwf@szu.edu.cn
[6]e-mail: scruan@szu.edu.cn

Received 17 May 2018; revised 16 July 2018; accepted 17 July 2018; posted 13 August 2018 (Doc. ID 331812); published 7 September 2018

Near infrared light-controlled release of payloads from ultraviolet-sensitive (UV-sensitive) polymer hydrogels or nanocarriers is one of the most promising strategies for biotherapy. Here, we propose the concept of light activation of $NaYF_4$:20%Yb, 2%Tm nanocrystals (NCs). $NaYF_4$:20%Yb, 2%Tm NCs are synthesized by a solvothermal method. Effective upconversion luminescence from $NaYF_4$:20%Yb, 2%Tm NCs excited by a continuous wave (CW) 980 nm laser is obtained. The $NaYF_4$:20%Yb, 2%Tm NCs are then used as a laser gain medium and sandwiched between Al and quartz reflectors to form laser microcavities. UV and blue upconverted random lasing is obtained from the laser microcavities. Hence, we verify explicitly that the $NaYF_4$:Yb, Tm NCs support UV and blue upconversion random lasing via a 980 nm nanosecond laser excitation. Our work provides what we believe is a new concept for precision and localized cancer therapy by external light excitation.

OCIS codes: (140.3380) Laser materials; (140.3613) Lasers, upconversion; (140.3945) Microcavities; (140.3610) Lasers, ultraviolet.

https://doi.org/10.1364/PRJ.6.000943

1. INTRODUCTION

Lanthanide-doped upconversion nanocrystals (UCNCs) have tremendous applications in multicolor three-dimensional displays, photovoltaic devices, solar cell technology, nanoscale thermometry, data storage, and bioimaging because of their unique upconversion luminescence properties [1–5]. Recently, UCNCs have been used as a light converter to enable near-infrared (NIR) light-controlled release of payloads from ultraviolet-sensitive (UV-sensitive) polymer hydrogels or nanocarriers [6–8]. By charging UCNCs within UV-sensitive systems, the nanocrystals act as an inside UV light source and emitted UV photons under NIR excitation can be absorbed by the photosensitive polymer, leading to the polymer carrier's disintegration and activating the photochemical reaction. A photosensitizer can convert light into heat that melts and softens drug-loaded hydrogel-based nanostructures. On the other hand, the high-power UV laser light emitted from UCNCs can also expect to kill the localized cancer cells and thus to achieve the biotherapy application [9]. This NIR excitation takes the place of UV light excitation, which is of great importance for light-controlled biomedical applications because there is less damage to healthy cells and enhanced tissue penetration. In this specific application, small-sized UCNCs are highly desirable because their encapsulation by UV-sensitive polymer nanocarriers (e.g., micelles and vesicles) may be easier than the generally used large particles. Therefore, the development of UV lasers emitted from small UCNCs that display efficient upconversion emission under NIR excitation is highly desirable.

The phenomenon that forms a random optical path through scattering in the grain boundaries of the random media is called the random lasing phenomenon, and it leads to the random distribution of lasing modes compared to defined lasing modes in conventional lasers [10]. In random lasers, the laser gain media are dependent strongly on the light interaction with the unordered amplifying medium and the scattering strength [11–13]. Recently, random lasers have attracted a lot of interest

due to simple device structures, easy fabrication, small size, low cost, and their potential application in various fields, in particular, water purification and speckle-free imaging [14–18]. Random lasers have been realized in different systems, including conjugated polymer films, organic dye-doped gel films, silver nanoparticles, ZnO films, and TiO_2 films [19–23]. However, $NaYF_4$-based random lasers have rarely been demonstrated.

To address these issues, uniform $NaYF_4$:20%Yb, 2%Tm NCs were synthesized by a solvothermal method [24,25] and their room temperature upconversion emission properties were systematically investigated. Efficient upconversion luminescence from $NaYF_4$:20%Yb, 2%Tm NCs pumped by a continuous-wave (CW) 980 nm laser was obtained. Furthermore, the $NaYF_4$:20%Yb, 2%Tm NCs film was used as a random laser gain medium to demonstrate random lasing by planar microcavities, which hold strong optical confinement with lower cavity losses and a high quality factor [26]. The nanosecond pulsed laser with high peak intensity was used to achieve high gain from the $NaYF_4$:20%Yb, 2%Tm NCs. As a result, this work can facilitate the use of $NaYF_4$:20%Yb, 2%Tm NCs in biologic therapy.

2. EXPERIMENT

In a typical solvothermal method for the synthesis of high-quality $NaYF_4$:20%Yb, 2%Tm NCs, YCl_3, $YbCl_3$, and $TmCl_3$ were added to a 100 mL three-neck round-bottom flask containing 3 mL oleic acid (OA) and 15 mL 1-octadecene (ODE) [25]. The solution was stirred and heated to 160°C for 30 min to form homogeneous lanthanide oleate complexes, and then cooled down to 50°C. Afterward, a solution of NaOH and NH_4F dissolved in 10 mL methanol was added into the flask and stirred quickly for 30 min at 50°C. Subsequently, the solution was heated to 120°C for 30 min to evaporate methanol from the reaction mixture completely, then heated to 300°C in an argon atmosphere for 60 min and then cooled to room temperature naturally. The resulting nanocrystals were precipitated from the solution by the addition of ethanol, and collected by centrifugation. Then the precipitates were washed with an ethanol and water (1∶1 volume ratio) mixture three times and finally redispersed in cyclohexane for further experiments.

High-resolution transmission electron microscope (HR-TEM) images of the $NaYF_4$:Yb/Tm NCs were characterized by a JEOL JEM-2100F with an acceleration voltage of 300 kV. The phase identification was performed by a Rigaku SmartLab Intelligent X-ray diffractometer (XRD) with filtered Cu-Kα radiation ($\lambda = 0.15406$ nm, operating at 45 kV and 200 mA). The step scan covered the angular range from 10° to 80° in steps of 0.04°. Upconversion emission spectra were obtained with an Ocean Optics Maya2000 Pro spectrometer by a power-adjustable CW 980 nm laser diode pumping. The lasing characteristics of $NaYF_4$:Yb/Tm NCs were investigated by third harmonic generation from a YAG pulsed laser (355 nm, 10 Hz) with an optical parameter oscillator to expand the YAG laser to different excitation wavelengths. The lasing spectra were recorded by a Horiba iHR 320 spectrometer. The laser beam was focused on the sample by a 50 mm focal length optical lens and 800 μm laser spot diameters. All of the measurements were conducted at room temperature.

3. RESULTS AND DISCUSSIONS

A. Morphology and Structural Characterization

The detailed structure of the $NaYF_4$:Yb, Er NCs was recorded by using TEM and HR-TEM, shown in Fig. 1(a). The TEM images reveal that the $NaYF_4$:Yb, Er NCs are in a nearly spherical shape and uniformly distributed. These regular NCs, which display high-quality, uniform morphology, are likely to be self-assembled on the TEM grid because of the interaction of their surface hydrophobic surfactants (i.e., OA). From the HR-TEM image, we can clearly distinguish lattice fringes on the individual crystals, which indicates that the NCs are highly crystalline in nature and have structural uniformity. The interplanar distance of the NCs was measured to be about 0.5 nm, which matched to a (100) lattice plane of the hexagonal $NaYF_4$ structure (0.515 nm, JCPDS # 16-0334). The selected area electron diffraction (SAED) and size distribution of NCs are given in Figs. 1(b) and 1(c), respectively. The SAED pattern of the NCs further demonstrates a perfect hexagonal crystal structure, which is in good agreement with the XRD results presented in Fig. 1(d). The $NaYF_4$:Yb, Tm NCs with size distribution between 14 and 30 nm and average size about 22 nm without aggregation were observed. The crystal structures and phase purity of the samples were examined by XRD, which demonstrates that the sample was highly crystalline in nature. The peak positions and intensities of the sample pattern well correspond to the reported and calculated patterns for 100, 110, 101, 200, 111, 201, 210, 002, 300, 211, 102, 112, 220, 202, 310, 311, 312, and 302 reflections of hexagonal phase structure β-$NaYF_4$ (JCPDS#16-0334) [27]. No cubic phase diffraction peaks or other impurities were detected, which revealed that pure β-$NaYF_4$ had been fabricated. It can be seen that the diffraction peaks of the β-$NaYF_4$ samples are very strong and sharp, which indicates that synthesized products with high crystallinity have been obtained at the high temperature treatment (300°C). Higher crystallinity is very important for phosphors generally due to less traps and stronger luminescence.

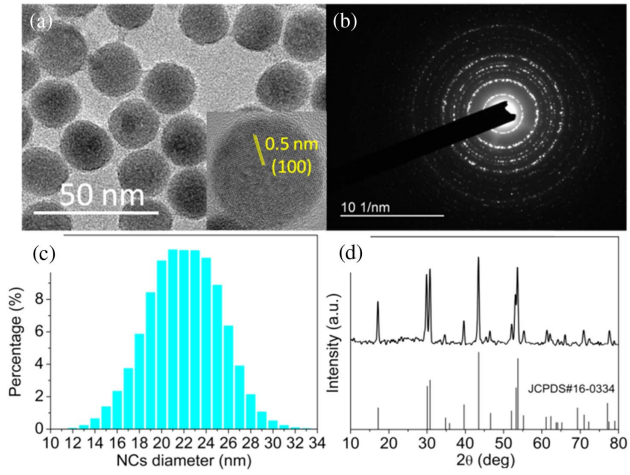

Fig. 1. (a) TEM image and HR-TEM image (inset), (b) SAED pattern, (c) size distribution, and (d) XRD pattern of the $NaYF_4$:Yb, Tm NCs.

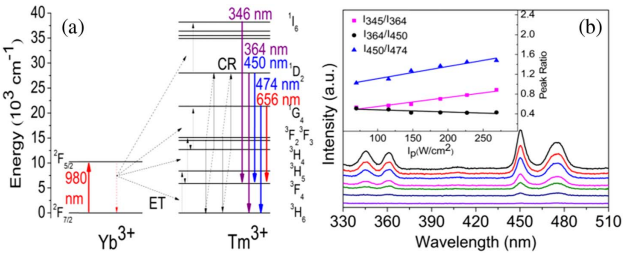

Fig. 2. (a) Schematic diagram of energy levels and transitions of Yb^{3+} and Tm^{3+} ions by 980 nm pumping. (b) Upconversion luminescence spectra of $NaYF_4$:20%Yb, 2%Tm by 980 nm excitation at room temperature. The inset of (b) is the plot of peak intensity ratios, I_{345}/I_{364}, I_{346}/I_{450}, and I_{450}/I_{474} versus I_p.

B. Upconversion Luminescence Properties

The energy transfer (ET) and excited state absorption (ESA) are efficient UC mechanisms in RE^{3+}-doped UC materials. Because Yb^{3+} ions have a larger absorption cross section at 980 nm, the ET from Yb^{3+} to Tm^{3+} plays a key role in UC processes in Yb^{3+}-sensitized Tm^{3+}-doped materials. The schematic diagram of energy levels and transitions of Yb^{3+} and Tm^{3+} ions by 980 nm pumping is shown in Fig. 2(a). According to the schematic diagram of upconversion processes, the $^1D_2$ level of Tm^{3+} ions cannot be directly populated by an ET from excited Yb^{3+} to the Tm^{3+} ions in the $^1G_4$ level due to the large energy mismatch (~3500 cm^{-1}). Hence, the cross-relaxation processes of $^3F_{2,3} + {}^3H_4 \rightarrow {}^3H_6 + {}^1D_2$ between Tm^{3+} ions may alternatively play an important role in populating the $^1D_2$ level. The upconversion luminescence spectra of $NaYF_4$:Yb, Tm NCs with different pump power under CW 980 nm excitation at room temperature are presented in Fig. 2(b). The nanocrystals dispersed in cyclohexane were held by a quartz cuvette for the photoluminescence (PL) experiment. According to the energy level diagram shown in Fig. 2(a), there were four dominant emission peaks centered at 345, 360, 450, and 474 nm that correspond to the transitions between energy levels $^1I_6 \rightarrow {}^3F_4$, $^1D_2 \rightarrow {}^3H_6$, $^1D_2 \rightarrow {}^3F_4$, and $^1G_4 \rightarrow {}^3H_6$ of Tm^{3+} ions, respectively. It is observed that the upconversion emission intensity increases with an increase in the excitation power at 980 nm. The inset of the Fig. 2(b) gives the dependence of peak intensity ratios, I_{345}/I_{364}, I_{346}/I_{450}, and I_{450}/I_{474} versus excitation power, I_p. It can be seen that the value of I_{346}/I_{450} remains insensitive to I_p, and both I_{346} and I_{450} simultaneously saturate with increasing of I_p. This can be expected because the optical gain of I_{346} and I_{450} consumes the same pool of

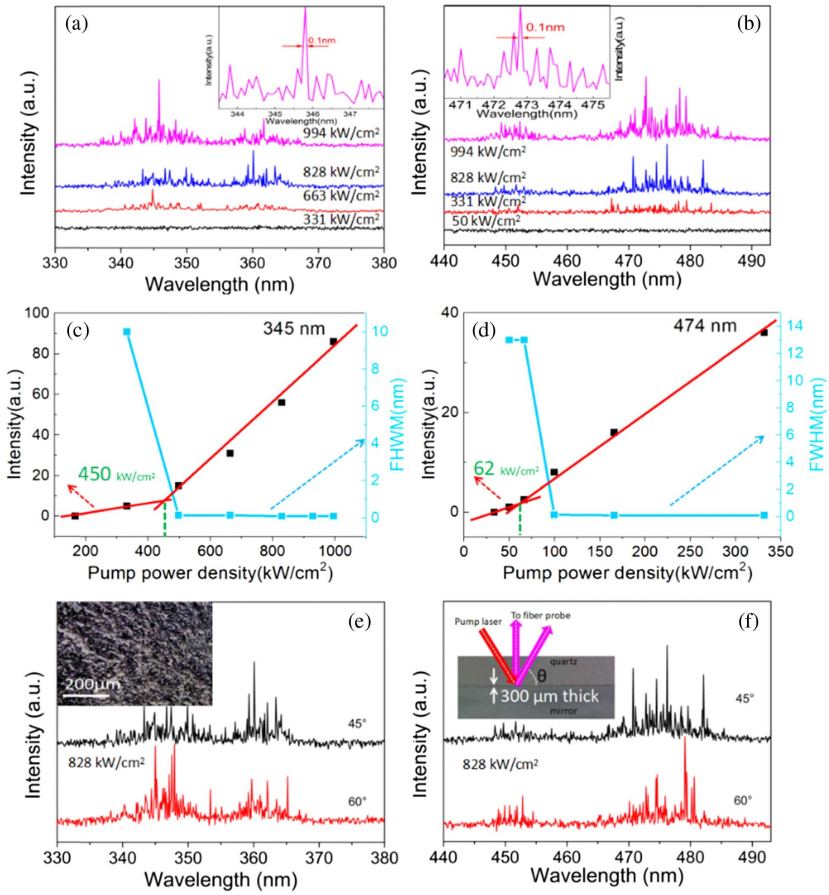

Fig. 3. Emission spectra versus different excitation power at (a) 345 nm and (b) 474 nm. The insets of (a) and (b) are the FWHM of the emission spectra of NCs lasers. (c) and (d) Output intensity and FWHM of the emission spectra at 345 nm and 474 nm versus different pump power density. Emission spectra at different observation angles at (e) 345 nm and (f) 474 nm. The left inset of (e) is the optical microscope image of the $NaYF_4$:20%Yb, 2%Tm NCs film. The inset of (f) is the sandwich structure of the proposed $NaYF_4$:Yb, Tm NCs lasers.

upconversion population (i.e., $^1D_2$ excited state). However, their emission intensity is different owing to a difference in differential gain (i.e., stimulated emission cross section).

C. $NaYF_4$:Yb, Tm NCs Lasers

The random lasing action from $NaYF_4$:Yb, Tm NCs was studied using 980 nm nanosecond laser (6 ns, 10 Hz) excitation. We designed planar microcavities that sandwich the $NaYF_4$:Yb, Tm NCs film with 300 μm thickness between a quartz plate and an aluminum (Al) mirror (Al-coated glass substrate). The mirrors are used to improve the longitudinal confinement of light and achieve optical feedback along the laser microcavities. The pump laser beam is focused on an 800 μm diameter spot by a 50 mm focal lens. The small beam size promotes the lateral confinement of the emission light so that a planer microcavity can be formed [26]. Laser emission is detected from the side of the quartz mirror. The spectral evolution with increasing pumping power density and the emission peak intensity as a function of the pumping power are shown in Fig. 3. Figures 3(a) and 3(b) depict the emission spectra of the $NaYF_4$:Yb, Tm NCs laser around 345 and 474 nm. Only the weak spontaneous emission band centered at ~345 nm can be detected for the film of the NCs when the excitation power is well below the excitation threshold value of ~450 kW/cm^2, namely, the kink of the light–light curve, as shown in Figs. 3(a) and 3(c). Similarly, as shown in Figs. 3(b) and 3(d), the weak spontaneous emission band centered at ~474 nm is obtained when the excitation power is below the excitation threshold value of ~62 kW/cm^2. To further confirm the random lasing action, the full width at half maximum (FWHM) at different pump power densities is also shown in Figs. 3(c) and 3(d). The FWHM acutely decreases from 10 to 5 nm at 345 nm and 13 to 6 nm at 474 nm, respectively, when the pump power increases. In addition, more sharp peaks further emerge from the emission spectra when the pump power increases. However, once the random lasing action is achieved, the lasing wavelength and lasing intensity are determined by the resonance of the microcavity, making the formation of many narrow peaks [28]. The $NaYF_4$:Yb, Tm NCs laser spectra show several sharp peaks with line widths less than 0.1 nm when the excitation power is larger than the threshold value. It also can be observed from Figs. 3(a) and 3(b) that the lasing modes are distributed randomly in the lasing spectra because the $NaYF_4$:Yb, Tm NCs are aggregated with each other in the gain film after solvent evaporation. The aggregation results in light scattering in the gain medium [29]. As shown in Figs. 3(a) and 3(b), the lasing spectra do not reveal the presence of Fabry–Perot modes as the mode spacing is distributed nonuniformly over the emission spectrum. This phenomenon can also be verified by different lasing spectra obtained from different detection angles, as shown in Figs. 3(e) and 3(f). It is shown clearly that the recorded emission spectra are varied at different angles because the NCs are randomly distributed between the sandwich structure so that the corresponding scattering strength is strongly dependent on the detection angle [29]. The left inset of Fig. 3(e) is the optical microscope image of the $NaYF_4$:20%Yb, 2%Tm NCs, which verifies that the random light scattering occurs in the $NaYF_4$:Yb, Tm NCs gain medium film. As results, it is verified that $NaYF_4$:Yb, Tm NCs film supports coherent random lasing action.

4. CONCLUSIONS

We have demonstrated UV and blue light upconversion random lasing from $NaYF_4$:Yb, Tm NCs. It is noted that lasing emission with a peak wavelength of ~345 nm and ~474 nm under 980 nm nanosecond excitation is obtained from the $NaYF_4$:20%Yb, 2%Tm NCs film sandwiched between an Al mirror and a quartz mirror. This longitudinal optical confinement is achieved via the optical feedback between the two interfaces. Hence, the formation of a low-loss planar microcavity can support the random lasing action at room temperature. The discrete sharp peaks show the formation of a closed light loop path, with a linewidth ~0.1 nm achieved from the emission spectra. The variation of the emission spectra with different detection angles verifies the support of random lasing action. As a result, our proposed $NaYF_4$:20%Yb, 2%Tm NCs, for which the realization of upconversion random lasing has been verified unambiguously, are potential optical gain media suitable for optical applications.

Funding. Natural Science Foundation of SZU (827-000130); National Natural Science Foundation of China (NSFC) (51502176, 61378071); Science and Technology Projects of Shenzhen (JCYJ20150324141711618, JCYJ20160427105041864, JCYJ20170818101651195, JSGG20160429114438287).

REFERENCES

1. C. Yan, H. Zhao, D. F. Perepichka, and F. Rosei, "Lanthanide ion doped upconverting nanoparticles: synthesis, structure and properties," Small **12**, 3888–3907 (2016).
2. L. E. Mackenzie, J. A. Goode, A. Vakurov, P. P. Nampi, S. Saha, G. Jose, and P. A. Millner, "The theoretical molecular weight of $NaYF_4$: RE upconversion nanoparticles," Sci. Rep. **8**, 1106 (2018).
3. Y. Cho, S. W. Song, S. Y. Lim, J. H. Kim, C. R. Park, and H. M. Kim, "Spectral evidence for multi-pathway contribution to the upconversion pathway in $NaYF_4$:Yb^{3+}, Er^{3+} phosphors," Phys. Chem. Chem. Phys. **19**, 7326–7332 (2017).
4. M. Xu, D. Chen, P. Huang, Z. Wan, Y. Zhou, and Z. Ji, "A dual-functional upconversion core@shell nanostructure for white-light-emission and temperature sensing," J. Mater. Chem. C **4**, 6516–6524 (2016).
5. G. Chen, H. Qiu, P. N. Prasad, and X. Chen, "Upconversion nanoparticles: design, nanochemistry, and applications in theranostics," Chem. Rev. **114**, 5161–5214 (2014).
6. B. Yan, J.-C. Boyer, N. R. Branda, and Y. Zhao, "Near-infrared light-triggered dissociation of block copolymer micelles using upconverting nanoparticles," J. Am. Chem. Soc. **133**, 19714–19717 (2011).
7. B. Yan, J.-C. Boyer, D. Habault, N. R. Branda, and Y. Zhao, "Near infrared light triggered release of biomacromolecules from hydrogels loaded with upconversion nanoparticles," J. Am. Chem. Soc. **134**, 16558–16561 (2012).
8. F. Shi and Y. Zhao, "Sub-10 nm and monodisperse b-$NaYF_4$:Yb, Tm, Gd nanocrystals with intense ultraviolet upconversion luminescence," J. Mater. Chem. C **2**, 2198–2203 (2014).
9. L. Liang, A. Care, R. Zhang, Y. Lu, N. H. Packer, A. Sunna, Y. Qian, and A. V. Zvyagin, "Facile assembly of functional upconversion nanoparticles for targeted cancer imaging and photodynamic therapy," ACS Appl. Mater. Interfaces **8**, 11945–11953 (2016).
10. B. Redding, M. A. Choma, and H. Cao, "Speckle-free laser imaging using random laser illumination," Nat. Photonics **6**, 355–359 (2012).

11. L. Florescu and S. John, "Photon statistics and coherence in light emission from a random laser," Phys. Rev. Lett. **93**, 013602 (2004).
12. A. L. Burin, H. Cao, and M. A. Ratner, "Understanding and control of random lasing," Phys. B Condens. Matter **338**, 212–214 (2003).
13. A. Yadav, L. Zhong, J. Sun, L. Jiang, G. J. Cheng, and L. Chi, "Tunable random lasing behavior in plasmonic nanostructures," Nano Converg. **4**, 1 (2017).
14. D. S. Wiersma and S. Cavalieri, "Light emission: a temperature-tunable random laser," Nature **414**, 708–709 (2001).
15. R. C. Polson and Z. V. Varden, "Random lasing in human tissues," Appl. Phys. Lett. **85**, 1289–1291 (2004).
16. D. S. Wiersma, "The physics and applications of random lasers," Nat. Phys. **4**, 359–367 (2008).
17. Q. Song, S. Xiao, Z. Xu, V. M. Shalaev, and Y. L. Kim, "Random laser spectroscopy for nanoscale perturbation sensing," Opt. Lett. **35**, 2624–2626 (2010).
18. Q. Song, Z. Xu, S. H. Choi, X. Sun, S. Xiao, O. Akkus, and Y. L. Kim, "Detection of nanoscale structural changes in bone using random lasers," Biomed. Opt. Express **1**, 1401–1407 (2010).
19. S. V. Frolov, W. Gellermann, M. Ozaki, K. Yoshino, and Z. V. Vardeny, "Cooperative emission in conjugated polymer thin films," Phys. Rev. Lett. **78**, 729–732 (1997).
20. R. C. Polson and Z. V. Vardeny, "Organic random lasers in the weak-scattering regime," Phys. Rev. B **71**, 045205 (2005).
21. G. D. Dice, S. Mujumdar, and A. Y. Elezzabi, "Plasmonically enhanced diffusive and subdiffusive metal nanoparticle-dye random laser," Appl. Phys. Lett. **86**, 131105 (2005).
22. S. F. Yu and E. S. Leong, "High-power single-mode ZnO thin-film random lasers," IEEE J. Quantum Electron. **40**, 1186–1194 (2004).
23. Z. Wang, X. Meng, A. V. Kildishev, A. Boltasseva, and V. M. Shalaev, "Nanolasers enabled by metallic nanoparticles: from spasers to random lasers," Laser Photon. Rev. **11**, 1700212 (2017).
24. H.-X. Mai, Y.-W. Zhang, R. Si, Z.-G. Yan, I.-D. Sun, L.-P. You, and C.-H. Yan, "High-quality sodium rare-earth fluoride nanocrystals: controlled synthesis and optical properties," J. Am. Chem. Soc. **128**, 6426–6436 (2006).
25. Z. Li and Y. Zhang, "An efficient and user-friendly method for the synthesis of hexagonal-phase NaYF(4):Yb, Er/Tm nanocrystals with controllable shape and upconversion fluorescence," Nanotechnology **19**, 345606 (2008).
26. Q. Song, L. Liu, S. Xiao, X. Zhou, W. Wang, and L. Xu, "Unidirectional high intensity narrow-linewidth lasing from a planar random microcavity laser," Phys. Rev. Lett. **96**, 033902 (2006).
27. L. M. Jin, X. Chen, C. K. Siu, F. Wang, and S. F. Yu, "Enhancing multi-photon upconversion from $NaYF_4$:Yb/Tm@$NaYF_4$ core shell nanoparticles via the use of laser cavity," ACS Nano **11**, 834–849 (2017).
28. H.-I. Lin, K.-C. Shen, Y.-M. Liao, Y.-H. Li, P. Perumal, G. Haider, B. H. Cheng, W.-C. Liao, S.-Y. Lin, W.-J. Lin, T.-Y. Lin, and Y.-F. Chen, "Integration of nanoscale light emitters and hyperbolic metamaterials: an efficient platform for the enhancement of random laser action," ACS Photon. **5**, 718–727 (2018).
29. X. Xu, W. Zhang, L. Jin, J. Qiu, and S. F. Yu, "Random lasing in Eu(3)(+) doped borate glass-ceramic embedded with Ag nanoparticles under direct three-photon excitation," Nanoscale **7**, 16246–16250 (2015).